Final Draft
Manuscript available at: https://doi.org/10.1061/(ASCE)ST.1943-541X.0003063
Full citation: Tumbeva, MD and Thrall, AP (2021) "Modular Connector for Resilient Grid Shell Structures." Journal of Structural Engineering, 147(8), 04021115

Modular Connector for Resilient Grid Shell Structures

Mirela D. Tumbeva, S.M.ASCE[1]; Ashley P. Thrall, A.M.ASCE[2]

ABSTRACT

In the design, fabrication, and erection of grid shells, a major challenge is the nodal connector between members. Designers typically select a structure's form and then design the nodal connectors to meet geometric and structural demands. However, this can lead to complicated connections that are difficult and expensive to fabricate. Each connector is also often unique. To address these challenges, this paper investigates a new approach in which a novel modular connector is designed for ease of fabrication and erection, and then structural forms are developed that use the connector repeatedly to join wide flange steel members via splice connections in double shear. This approach "modularizes" the nodal connector, which is a prefabricated, steel connector with starter segments that include webs and flanges. The flanges and webs of the modular connector and the members are joined independently thus achieving a moment-resisting connection. This facilitates truss-like, membrane-like, or beam-like behavior, as well as allows load to be redistributed in the case of sudden member loss or replacement thereby providing enhanced resiliency. Variability in form is achieved by bending the flange splice plates. This paper investigates the modular connector for free-form undulating grid shells and for rational structural forms developed through a proposed form-finding methodology. The proposed methodology relies on thrust network analysis coupled with geometric and structural constraints. The promise of the modular connector and the proposed methodology is demonstrated through finite element numerical analyses.

Key Words: Modular construction, Connection design, Grid shells, Form-finding, Steel structures

[1]Ph.D. Candidate, Kinetic Structures Laboratory, Department of Civil and Environmental Engineering and Earth Sciences, University of Notre Dame, Notre Dame, IN 46556. E-mail: mtumbeva@nd.edu

[2]Myron and Rosemary Noble Associate Professor of Structural Engineering, Kinetic Structures Laboratory, Department of Civil and Environmental Engineering and Earth Sciences, University of Notre Dame, Notre Dame, IN 46556. (corresponding author) E-mail: athrall@nd.edu

Introduction

Shell structures (e.g., space frames, grid shell, domes) are appealing to architects and engineers due to their efficiency in spanning long distances while providing aesthetically pleasing forms. These systems can be continuous surfaces (e.g., thin shell concrete structures) or, as in the case of grid shells, be comprised of discrete elements (members and nodal connectors) following the geometry of a continuous surface. The geometry of grid shells can be categorized as free-form or form-found. Free-form grid shells are typically developed through computer aided software primarily following a geometrical formulation, as opposed to prioritizing a structural behavior. However, with the advancement in computational capabilities and manufacturing technologies, the ability to generate and analyze a wide range of shapes has enabled a growth in popularity of these free-form structures. Knippers and Helbig (2009) presented two examples of free-form glazed structures including the design process as well as fabrication and construction strategies. Schlaich and Schober (2005) described the development of free-form glazed structures using triangular and quadrilateral glass panels based on their long experience in design. Glymph et al. (2004) proposed a parametric strategy for the design of the Jerusalem Museum of Tolerance which is comprised of multiple free-form glass structures. Using geometric principles incorporated into computational models, Glymph et al. (2004) were able to achieve the structural form using quadrilateral glass panels. Alternatively, the shape of rational (i.e., based on structural performance) grid shells can be developed through numerical form-finding methods. Form-finding is a process that solves a system of equilibrium equations to find an optimized structural shape based on input parameters including: (1) initial geometry (or mesh), (2) boundary conditions, and (3) external loading. These input parameters can also be controlled to allow for different grid shells to be explored (Adriaenssens et al., 2014). Numerical form-finding methods such as Force Density Method (FDM) (Linkwitz and Schek, 1971; Schek, 1974), Dynamic Relaxation (DR) (Day, 1965), and Thrust Network Analysis (TNA) (Block, 2009) have been successfully implemented in the development of rational structural forms. FDM has been mostly used for finding the form of pre-stressed cable-net roofs, hanging structures, and timber grid shells. Over the years, various modifications to the method have been introduced. For example, Ye et al. (2012) proposed a modified FDM for form-finding of membrane structures that, instead of prescribing the force densities, uses the membrane stresses and cables tension force as initial conditions. Sanchez et al. (2007) introduced a multi-step FDM for form-finding tensile membrane structures by adjusting the force densities to achieve a smooth or uniform stress distribution in the final equilibriated shape. Miki and Kawaguchi (2010) proposed an extension to the FDM based on the variational principle to address limitation of the original FDM when the structure is subjected to both tension and compression. The DR method was first introduced by Day (1965) as a new approach for solving structural problems such as portal frames, flat plates, and thick cylinders. DR was later adopted for form-finding of tension structures and grid shells (Barnes, 1988, 1999). Adriaenssens and Barnes (2001) developed a method based on DR for form-finding tensegrity structures with curved splines that incorporates the effect of the bending moments. Richardson et al. (2013) proposed a two-phase approach for the design of single layer grid shells that consists of developing the initial grid shell form through DR and using a genetic algorithm to optimize the grid topology. Bagrianski and Halpern (2014) proposed a new approach - Prescriptive Dynamic Relaxation - for form-finding compressive structures with initially prescribed member lengths. The TNA method was developed mostly for the design and analysis of masonry or concrete vaulted structures and is used for finding compression only structures (Block and Ochsendorf, 2007; Block, 2009). TNA has beeen modified and improved to include different constraints and make the form-finding algorithm faster and more robust (Fraternali, 2010; Panozzo et al., 2013; Marmo and Rosati, 2017; Liew et al., 2018). A thorough description of these methods can be found in Adriaenssens et al. (2014) and a comparison among these existing methods for the general case of discrete networks can be found in Veenendaal and Block (2012).

For both free-form and form-found grid shells, the state-of-the-practice in design is to choose the global shape of the structure first. Nodal connectors are typically considered last, with their geometry dictated by the form and sized to meet demands. This results in connections that are unique, inefficient, and difficult to fabricate. Each structure is designed as one-of-a-kind, leading to further inefficiencies. In contrast, this research advocates for a new paradigm in design: start with connectors that are designed for ease of fabrication and erection, and then develop an efficient structural form that is consistent with these connectors. This approach "modularizes" the nodal connector such that identical connectors can be used repeatedly throughout the structure and among many structures. This research specifically introduces a "modular connector" for grid shell structures which is a prefabricated, steel nodal connector that is designed for ease of fabrication (Figure 1A). Standard rolled wide flange members serve as members, joined by modular connectors, to achieve free-form or form-found steel grid shells (Figure 1C and D). Specifically, the modular connector is comprised of top and bottom flange plates, as well as web plates, all cut from flat steel plate. The components are welded to one another and to a standard round hollow structural section (HSS) at the center. The open geometry of the connector facilitates the welding process. The modular connector includes straight starter segments for connection to the wide flange members. The flanges and webs of the connector and the members are joined independently through bolted splice connections in double shear (Figure 1B). This results in a moment-resisting connection that enables truss-like, membrane-like, or beam-like behavior and provides enhanced resiliency as member loss can be tolerated. Using only bolted connections (i.e., no field welding) provides savings in erection costs. Various structural forms (to improve efficiency or to satisfy architectural constraints) are achieved by using bent flange splice plates, which can be the adjustable bolted steel plate connection (Gerbo et al., 2016, 2018, 2020a,b). These bent flange plates enable the components to be joined at an angle, γ. The modular connector and wide flange members are also designed for ease of transportation in standardized by the International Standard Organization shipping containers (ISO containers, hereafter). Ultimately, this paper proposes a new kit-of-parts for the design and fabrication of a wide variety of steel grid shells comprised of (1) modular connectors, (2) standard wide flange sections, and (3) bolted splice connections.

Tumbeva et al. (2021) proposed an analogous, but different, approach for the modular construction of steel bridges. In Tumbeva et al. (2021), a two-dimensional (2D) modular joint is proposed which is comprised of cold bent flange plates, flat flange plates, and a web (Figure 2A). This modular joint replaces the function of a gusset plate with a more reliable connection and enables the upper chord, lower chord, and diagonal members to be standard rolled wide flange sections (Figure 2B). The modular connector introduced in this paper, as well as the modular joint proposed in Tumbeva et al. (2021), represent a new paradigm in modular construction, in which the connection between members becomes the module and structural forms are derived to be consistent with the modules.

Extensive research has been performed on developing and investigating the behavior of nodal connectors for grid shells and spatial structures, with a particular focus on single layer grid shells. For example, Feng et al. (2015) experimentally and numerically investigated the behavior of modified conventional bolted joints for cable-braced grid shells with a particular focus on the joint stiffness and failure mechanism. Seifi et al. (2018) proposed two different approaches for simplifying the design and analysis of nodal connectors for grid shells that have improved mechanical properties and can be 3D printed. These approaches are more focused on the design of nodal connectors that are specific to a project, as opposed to promoting a modular kit-of-parts. Ma et al. (2016a,b) proposed a new semi-rigid bolt-column joint (BC), comprised of a hollow column node, bolts, and a cone part for connection to rectangular hollow or wide flange sections. The BC joint achieves the geometry of the grid shell by positioning the entire joint at a desired angle. Oh et al. (2016) numerically investigated a new hollow spherical connector - FREE node - to determine an efficient node shape while considering the connector's failure mode and stiffness. The FREE node is comprised of hollow sphere, sub-wings, and wings that can connect hollow sections through bolting. To achieve different angles however, welding of the members directly to the hollow sphere may be required. Many patents have been developed for various universal connections [e.g. Rochas (2014), Allred et al. (2013), Boots (2008), Reynolds et al. (2006)]. In comparison to existing technologies, the connector proposed in this paper (1) enables members to be joined at different angles thus achieving wide variability in structural form, (2) can join many different standard wide flange sections for high efficiency and adaptability for demand, and (3) facilitates a more reliable, moment-resisting connection for enhanced resiliency.

OBJECTIVES AND SCOPE

This research addresses a major challenge in the design, fabrication, and erection of grid shells: nodal connectors. This research introduces a novel modular connector that retains the advantages of modularity (i.e., that a single, prefabricated component can be repeated throughout a structure and among many structures, leading to cost savings and time efficiencies) while being able to achieve free-form and form-found grid shells using standard sections as members and providing enhanced resiliency through moment-resisting connections. The specific objectives of this paper are to: (1) develop the geometry of the modular connector for free-form and form-found grid shells, (2) propose a form-finding methodology to achieve rational, compression-only grid shells that meet geometric and structural criteria, and (3) demonstrate the promise of this approach through finite element (FE) numerical analyses. Ultimately this research presents a new paradigm in design in which nodal connectors are developed for ease of design, fabrication, and erection and structural forms, consistent with the constraints of the nodal connector, are chosen.

GEOMETRIC PARAMETERS OF THE MODULAR CONNECTOR

To develop the modular connector, the following parameters are defined (Figure 3): (1) number of starter segments, ns, (2) angle between starter segments, θ, (3) depth of the web plate, w, (4) flange width, f, (5) radius, R, and (6) starter segment length, d.

This research proposes a modular connector with six starter segments (ns = 6) to be able to join up to 6 members, thus generating a triangulated grid shell which is desirable to ensure global stability of the structure. Triangulation also enables flat planes of glass to be used between members to form the enclosed space. Analogous modular connectors with different number of starter segments could also be considered. With six starter segments and the choice that the starter segments are evenly spaced, the angle between starter segments, θ is then $60°$.

The depth of the web plate, w is selected such that the modular connector can join a range of standard wide flange sections, thereby allowing greater variability in structural forms. For standard wide flange members with the same nominal depth (i.e., sections with the same WXX designation, where XX refers to the nominal depth), the web depth (i.e., the section depth minus the thickness of the two flanges) is approximately the same as a result of the steel rolling fabrication process. This paper specifically focuses on a set of ten W14 wide flange sections between W14x109 and W14x257 (AISC, 2011). Therefore, the depth of the web plate, w of the modular connector is selected to be 320 mm (12.6 in.) that is the average web depth of the selected set of wide flange sections. A designer could choose other depths corresponding to other types of wide flange sections. Alternatively, fill plates could be used. Note that, when bent flange splice plates are used, fill plates are required as the modular connectors and members are connected at an angle, γ (Figure 1B). The modular connector flange width, f is 406 mm (16 in.), which is selected to be on the upper limit of the flange widths of the considered wide flange sections.

The radius, R is chosen to be 508 mm (20 in.). A large radius is beneficial as it reduces stress concentrations at the curved region of the flange plates of the connector as well as increases the cross sectional area of the flange. The starter segment length, d is chosen to be 229 mm (9 in) as a minimum value to facilitate a bolted splice connection. The length of each of the web plates, e can be calculated as follows:

$$e = d + \frac{(f/2) + R}{\tan \frac{\theta}{2}} - c \tag{1}$$

where c is the radius of the HSS section including its wall thickness.

The thickness of the flange plates and the web plates as well as the size of the HSS section can be determined based on demand.

FREE-FORM GRID SHELLS

Free-form grid shells can be approximately achieved (i.e., any polygonalized version of the desired continuous shape) using the modular connector, wide flange members, and bolted splice plate connections. To achieve variability in depth, this approach relies on angle changes, γ between modular connectors and wide flange sections about a single axis orthogonal to the webs which is achieved through bent flange splice plates (Figure 1B). Angles about any other axis would be incompatible with this system. Thus, it is required that all modular connectors be parallel to one another. It can be envisioned that all modular connectors are projected onto a parallel, planar $(x - y)$ mesh to ensure this requirement (Figure 4A). For the θ = 60° modular connector with 6 starter segments, this mesh would be comprised of equilateral triangles (Figure 4A). Based on the desired structural form, the z-coordinate of each modular connector, relative to the planar $(x - y)$ mesh, is determined (Figure 4B). The designer can select the mesh size, h of the equilateral triangles in the planar mesh, and thus, the $x - y$ coordinates of the modular connectors, based on aesthetics, architectural constraints, and/or structural demand. Each of the modular connectors join wide flange members through splice plates (bent or flat). If the modular connectors are placed at every vertex, the grid shell is triangulated, which provides stability (without relying on the moment-resisting connections) and enables flat glass to be used between members to enclose the space. The moment-resisting connection could then be relied upon in the event of member loss or replacement. A designer need not place modular connectors at every vertex of the mesh or use members between every modular connector, thereby providing freedom for openings or architectural vision (Tumbeva et al., 2018).

PROPOSED METHODOLOGY FOR FORM-FOUND GRID SHELLS

While any free-form undulating structure can be achieved, a structure that carries primarily axial load is preferred from a structural efficiency perspective, as opposed to bending dominant behavior. This paper proposes a new methodology for achieving form-found grid shells that primarily carry axial compression and are consistent with the modular connector.

In the state-of-the-practice, designers typically select a form-finding technique depending on the structural material. The boundaries of the structure, boundary conditions, and external loads are prescribed, as well as an initial geometry (or mesh). The form is then found with little regard to the geometry of the nodal connections between elements. Often unique nodal connection geometries result, leading to the previously discussed challenges in design, fabrication, and erection.

Instead, this research advocates for using a form-finding technique that is well-suited to connections that are easy to fabricate and erect. In this case, the focus is on the modular connector. TNA is well-suited for grid shells comprised of modular connectors as it derives a compression-only (under one load scenario) grid shell, G from an equilibrated planar mesh, Γ and the positions of the "free" nodes are found only in a direction perpendicular to that mesh (Figure 5). The $x - y$ coordinates of these free nodes are defined by the initial mesh and thus, are not found. The "support" nodes represent boundary conditions, with their $x - y - z$ coordinates being prescribed by the user. Truss elements are used to span between nodes. Truss elements are used to span between nodes. The geometry of the modular connectors is neglected (i.e., they are simplified to be infinitesimal nodes that connect truss elements). In the general formulation of TNA, the planar mesh is generated by the user (Block and Ochsendorf, 2007; Block, 2009). As shown in Figure 5, the planar mesh in this research is the mesh of equilateral triangles that is necessary for the modular connector, as discussed in the prior section. For a user-defined mesh size, h and loading, the z-coordinate of the free nodes is found. Thus, the planar coordinates of the modular connector are retained and the structural depth is found. This approach is limited to extrusions from a flat plane, where all modular connectors are parallel to this flat plane (i.e., the equilibrated planar mesh, Γ).

This paper proposes a methodology for finding efficient (i.e., minimized weight) compression-only grid shells that are compatible with the modular connector and meet structural constraints on behavior as well as geometric requirements (Figure 6). Minimizing the self-weight also results in a system that is sufficiently light for ease of transportation and erection. Alternatively, other objectives could be considered such as fabrication or erection cost. The methodology could also be reformulated as a multi-objective optimization problem that includes material efficiency and cost. For a user-defined span length, S, the methodology investigates n number of different planar meshes comprised of equilateral triangles with mesh size, h. An iterative TNA procedure is used to find the form of the compression-only grid shell and evaluate the axial forces in the member. To develop the geometry of the structure, TNA relies on a scale factor, ξ, to be discussed later. For each combination of h and ξ, the iterative TNA procedure is carried out. The feasibility of each form is then evaluated through structural and geometric constraints. One lowest weight solution, corresponding to one value of ξ, will result for each mesh size, h. The methodology ultimately finds the lowest weight solution among all of the different mesh sizes, h. While Figure 6 gives an overview of the proposed methodology, Figure 7 provides a detailed flow-chart of this methodology for one value of h and ξ.

Within the proposed methodology, an iterative TNA procedure is performed (dark shaded region in Figure 7) to find a compression-only grid shell form (i.e., the z-coordinates of the free nodes) and calculate the axial forces in the members. TNA, as described in the next section, is able to find a compression-only form under a single, known load. In this research, the load includes the self-weight of the wide flange members, the self-weight of structural glass panels between members, and a snow load. The geometry and self-weight of the modular connectors is ignored for simplicity. A major contribution to the overall load and thus, the form of the final 3D grid shell, is the self-weight. However, this weight cannot be known until a form is found, as it is calculated based on the structure's geometry which changes depending on the load. Thus, this research uses an iterative approach in which the load and form are updated until convergence is achieved. Convergence is defined as the difference in the z-coordinates of each free node between two successive iterations being less than a user-defined limit.Note that, the starter segments of the modular connector introduce an eccentricity of loading. The methodology neglects this eccentricity, as well as the moment resisting connections between members, for the purpose of rapidly converging on form. However, it would need to be incorporated for design.

Prior to starting the iterative approach, a database of M number of standard wide flange sections is defined and the section size, B_a, where a = 1 ($a \leq M$), with the smallest weight per linear foot is selected (Figure 7). Then, the iterative approach begins by setting the z-coordinates of the free nodes, z_f^i to zero, where i is the iteration number and f refers to the free nodes. Using the coordinates z_f^i, the load, P^i is calculated. TNA is then used to find a new set of nodal coordinates z_f^{i+1}. To avoid an infinite number of iterations and to allow a form to be found, an upper limit on the nodal coordinates is imposed: $z_m = S/5$. If z_f^{i+1} exceeds the limit z_m, a form is not found for that combination of h and ξ. If $z_f^{i+1} \leq z_m$, the convergence criteria: $z_f^{i+1} - z_f^i \leq 0.001$, is then evaluated for each node. If convergence is not achieved, the magnitude of the load is updated based on the found form and another iteration is performed. If convergence is satisfied, the form of the grid shell is found and the methodology continues with evaluating the structural and geometric constraints (light gray shaded region in Figure 7)

To ensure stability, the methodology includes structural constraints related to member buckling and global system buckling. The member buckling constraint requires that the axial force, F in each member must be less than the compressive strength, U of that member (for its weak axis) expressed in vector form: $\vec{F} < \vec{U}$, where U is calculated by (AISC, 2011):

$$U = \phi S_{cr} A_g \tag{2}$$

where ϕ is the resistance factor (ϕ = 0.9), A_g is the cross sectional area of the member, and S_{cr} is the critical stress determined as:

$$\begin{aligned} S_{cr} &= \left[0.658^{\frac{F_y}{F_e}}\right] F_y \qquad \text{When} \quad \frac{KL_u}{r_g} \leq 4.71\sqrt{\frac{E}{F_y}} \\ S_{cr} &= 0.877 F_e \qquad \text{When} \quad \frac{KL_u}{r_g} > 4.71\sqrt{\frac{E}{F_y}} \end{aligned} \tag{3}$$

where F_y is the yield strength [F_y = 345 MPa (50 ksi)], E is the modulus of elasticity [E = 200 GPa (29000 ksi)], K is the effective length factor (K = 1), r_g is the radius of gyration about the weak axis of the wide flange member, and L_u is the unbraced length of the member. While the geometry of the modular connector is not modeled in the TNA analysis (truss elements are assumed to span between nodal coordinates), the unbraced length is taken as the actual length of the wide flange member between what would be modular connectors, L_m (Figure 1C). F_e is the elastic buckling stress calculated by:

$$F_e = \frac{\pi^2 E}{\left(\frac{KL_u}{r_g}\right)^2} \tag{4}$$

If the member buckling constraint is satisfied, the global system buckling constraint is evaluated, which requires that the smallest critical buckling load factor, λ_1, exceeds 1. λ_1 is determined by solving the generalized eigenvalue problem $\left[\bar{K_E} + \lambda \bar{K_G}\right] \vec{\psi} = 0$, in which $\bar{K_E}$ is the global linear elastic stiffness matrix, $\bar{K_G}$ is the global geometric stiffness matrix, and $\vec{\psi}$ is the eigenvectors. In the buckling analysis, the 3D structure is modeled with truss elements and the member axial forces calculated through the TNA iterative approach are used. The boundary conditions at the supported nodes are: translation restrained in x, y, and z directions, free rotation. If either structural constraint is not met, the section size is increased and the iterative TNA procedure is repeated. If the maximum section size (i.e., a=M) is investigated and still fails to meet the structural criteria, the methodology ends with no feasible solution for that combination of h and ξ.

Note that, although the methodology uses standard wide flange sections, it is also compatible with other section types (e.g., L-sections, hollow structural sections). However, if the sections are slender, Equation 3 would need to modified according to AISC (2011). The global system buckling constraint would not be affected by the change in section type as it assumes truss elements and the axial forces are determined prior to solving the eigenvalue problem.

If the structural constraints are met, a geometric constraint, related to transporting the kit-of-parts in an ISO shipping container with inner length, T = 12 m (39 ft 4 in.) is evaluated (ISO, 2013). The length of each member, L_m is required to be less than T. If this constraint is satisfied, a second geometric constraint, related to the adjustable bolted steel plate connection developed by Gerbo et al. (2016, 2018, 2020a,b), is evaluated. The behavior of the connection, comprised of flat or prebent flange plates that are bent further in the field via bolt tightening, was investigated for angle changes up to $35°$. Thus, the angles between the modular connectors and wide flange members, γ are limited to γ_m = $\pm 35°$. If either of the two geometric constraints is not met, then the methodology ends with no feasible solution for that combination of h and ξ.

Form-Finding and Analysis through TNA

This research uses TNA to find compression-only forms and to calculate the axial forces in the members. TNA, proposed by Block and Ochsendorf (2007) and Block (2009), is a 3D version of thrust line analysis developed for form-finding and analysis of masonry and concrete vaulted structures. The form (i.e., the z-coordinates of the free nodes) of a compression-only vault is found through planar ($x - y$) equilibrium (via reciprocal form, Γ and force, Γ^* diagrams, to be discussed later) and perpendicular (z-direction) equilibrium (Figure 5). The vault is modeled as a discrete network of truss elements with loads applied only at the nodes, in the z-direction. Each truss element is required to be in compression only. Based on TNA, Rippmann (2016) proposed a framework for the interactive design of funicular shell structures which resulted in the development of the digital design tool RhinoVAULT (Rippmann et al., 2012). This section presents a brief review of TNA and how it is used in this research, which unless stated otherwise, is adapted from Block (2009).

In this research, TNA is used to determine the z-coordinates of the free nodes of a three-dimensional (3D) compression-only grid shell, G for one loading condition, applied as point loads in the z-direction (Figure 5). The z-coordinates are found through evaluating the perpendicular (z-direction) equilibrium of the structure, G defined as follows:

$$\bar{C}_f^T(\bar{L}_{xy}^{-1}\bar{F}_{xy})\bar{C}\vec{z} - \vec{p_z} = 0 \tag{5}$$

where $\bar{C}$ is an m x n matrix that represents the connectivity between m number of members and n number of nodes as follows:

$$\bar{C}_{mn} = \begin{cases} +1 & \text{if member } m \text{ starts with higher index node } n \\ -1 & \text{if member } m \text{ ends with lower index node } n \\ 0 & \text{all other entries} \end{cases} \tag{6}$$

The matrix $\bar{C}$ can be divided into two parts: $\bar{C}_f$ and $\bar{C}_s$ corresponding to the free (f) and support (s) nodes, respectively. In Equation 5, $\bar{L}_{xy}$ is a diagonalized matrix containing the lengths of the projection of the truss elements (with lengths $\bar{L}$ in 3D) onto the $x - y$ plane (Figure 5). $\bar{F}_{xy}$ is a diagonalized matrix containing the $x - y$ component of the axial force in the members which is found through the planar $(x-y)$ equilibrium of the structure. It is calculated as follows:

$$\bar{F}_{xy} = \bar{L}^{*}_{xy}\xi \tag{7}$$

where the matrix $\bar{L}^{*}_{xy}$ is discussed in the following subsection. In Equation 5, $\vec{p_z}$ is a vector of the applied loads.

Equation 5 can then be solved for the z-coordinates of the free nodes, $\vec{z_f}$:

$$\vec{z_f} = \bar{D}_f^{-1}(\frac{1}{\xi}\vec{p_z} - \bar{D}_s\vec{z_s}) \tag{8}$$

where $\vec{z_s}$ is the vector of the z-coordinates of the support nodes and the matrices $\bar{D}_f$ and $\bar{D}_s$ are:

$$\bar{D}_f = \bar{C}_f^T(\bar{L}_{xy}^{-1}\bar{L}^{*}_{xy})\bar{C}_f \tag{9}$$

$$\bar{D}_s = \bar{C}_f^T(\bar{L}_{xy}^{-1}\bar{L}^{*}_{xy})\bar{C}_s \tag{10}$$

The diagonalized matrix, $\bar{F}$ containing the axial forces in each member is calculated by:

$$\bar{F} = \bar{L}\bar{L}_{xy}^{-1}\bar{L}^{*}_{xy}\xi \tag{11}$$

Reciprocal Form and Force Diagrams

The planar $(x-y)$ equilibrium in TNA is solved through reciprocal form, Γ and force, Γ^* diagrams (Figure 5).

Reciprocal diagrams have mainly been used to design and analyze statically determinate 2D funicular structures under loads applied at the nodes. For 2D structures, the form diagram, Γ is a funicular polygon representing the structure's geometry, with nodes that are numbered and spaces between members represented by capital letters (Figure 8). Its reciprocal force diagram, Γ^* graphically represents the internal forces in the members, where the length of each branch corresponds to a scaled magnitude of the force in the parallel member of the form diagram. For example, the magnitude of the force in the member connecting nodes 2 and 8 (between spaces A and B) in Figure 8A is related to the length of the a-b branch of the force diagram by the scale factor. Each of the closed polygons in the force diagram represents the static equilibrium of a node in the form diagram (Maxwell, 1864). The concept of reciprocal diagrams is extended for 3D structures in TNA by Block and Ochsendorf (2007) and Block (2009).

In TNA, the form diagram, Γ is the planar mesh from which the 3D structure, G is found (Figure 5). The planar equilibrium of Γ and thus, the planar equilibrium of G, is represented by the force diagram, Γ^*. The $x - y$ component of the axial force in the members, $\bar{F_{xy}}$ is calculated from Equation 7, where $\bar{L^*_{xy}}$ (Figure 5) is the length of the branches of the force diagram and ξ is the scale factor defined as force per length of the force diagram. This is used in TNA for solving the perpendicular equilibrium.

In this research, the form diagram, Γ is the planar mesh of equilateral triangles that is required for the modular connector. Depending on the span length, S and mesh size, h, there are two types of form diagrams: Γ_1 and Γ_2 (Figure 9). Both diagrams are developed by calculating the q number of inner members (solid grey lines in Figure 9) along the span length by: $q = S/h$, where q is rounded down to the next even integer. The length of the two boundary members along the span length, connecting nodes 5 and 6 respectively in Γ is: $b = (S - qh)/2$. To maintain the planar mesh of equilateral triangles, the number of inner members along lines 1-3, 2-4, 5-6 are the same and equal to q. If $q/2$ is even, then the form diagram is Γ_1. If $q/2$ is odd, the form diagram is Γ_2.

For either type of form diagram, an infinite number of force diagrams exist, each representing a state of planar equilibrium of the 3D structure and therefore, a unique grid shell form. Figure 9 shows the force diagrams, Γ_1^* and Γ_2^* developed for form diagrams, Γ_1 and Γ_2, respectively. There are different ways to obtain the force diagram such as drawing it manually, using optimization methods (Block, 2009), or through iteration and additional constraints as proposed by Rippmann (2016). In this research, both force diagrams are constructed in a similar way by starting with the center node of the form diagram. The force diagram is developed in a clockwise direction to ensure that all members are in compression. As this research aims for a modular approach where all members are the same section size, it is desirable that all members have the same magnitude of force. To achieve this, the inner branches in the force diagram (shown with solid grey line in Figure 9) are required to have an equal length.

This research also employs a tension ring at the boundary of the grid shell (shown as black dashed lines in Figure 9) to counteract the horizontal thrust that would be generated at the supports. The tension ring is represented in the force diagram, Γ^* by branches that connect the center node with each of the edge nodes. The parallel tension ring members in the form diagram, Γ are intersecting the boundary members at the support nodes. Thus, the length of the boundary members, except those connecting nodes 5 and 6, in the form diagram, Γ are determined from the polygons constructed by the boundary and tension ring members. For the force diagram, Γ^* to be comprised of closed polygons, the length of the boundary branches must be twice that of the inner branches. Note that in the force diagram type Γ_1^*, the length of the boundary branches corresponding to the boundary members with dashed light grey lines in the form diagram, Γ_1 is the same as the length of the inner branches (Figure 9A). In the force diagram, Γ^*, the length of the corner branches corresponding to the corner members in the form diagram, Γ (connecting nodes 1, 2, 3, and 4, shown with solid grey lines in Figure 9) is the same as the length of the inner branches. To form closed polygons, the edge branches in the force diagram, Γ^* intersect the boundary branches, thus, the length of the edge branches is found from the geometry of the constructed polygons.

As mentioned earlier, the force diagram, Γ^* is a graphical representation of the forces, with the length of a branch indicating the magnitude of the force. The factor ξ is the scale that relates the length of a branch to a force magnitude (Equation 7). Because the coordinates z_f are inversely proportional to ξ, a smaller scale factor ξ results in higher values of z_f and thus, a deeper grid shell form, G (Equation 8). For the same form diagram and load, by only varying the scale factor, ξ, an infinite number of grid shell forms can be developed. The inner branches of the force diagram, Γ^* are given a unit length and all other branches are related to that unit length as discussed above. The proposed form finding methodology considers a range of scale factors, ξ to be able to select an efficient (i.e., minimized material use) grid shell from a vast number of solutions, based on structural performance criteria as well as transportation requirements.

CASE STUDIES

The developed methodology is demonstrated through four case studies with span lengths: S_1 = 42.7 m (150 ft), S_2 = 53.3 m (175 ft), S_3 = 61 m (200 ft), and S_4 = 76.2 m (250 ft). To explore a wide range of forms, the mesh size, h varies between 6.1 m (20 ft) and h_{max} in increments of 0.305 m (1 ft), where $h_{max} = T + 2(e + c)$ = 15.1 m (49.7 ft). The limit, h_{max} is based on the requirement that each member be transported in an ISO container (with inner length, T), including also the dimensions of the joint. The scale factor, ξ ranges from 1 to 1,000 in increments of 10. Hence, a total of 3,000 possible solutions were investigated for each span. The database of standard wide flange sections includes all section sizes from W14x109 through W14x257 resulting in M = 10 (AISC, 2011). It is assumed that all members have the same section to promote modularity.

Two load combinations as per the American Society of Civil Engineers Minimum Design Loads and Associated Criteria for Building and Other Structures Standard ASCE 7-16 (ASCE/SEI, 2017) were considered: $I_1 = 1.4D$ and $I_2 = 1.2D + 1.6N$, where D is the dead load and N is the snow load. For each iteration of the TNA procedure, the larger of the two load cases was applied. The dead load, D includes the self-weight of the wide flange members and self-weight of a structural glass of 0.781 kN/m^2 (15 psf) which is assumed to span between members (AISC, 2011). The self-weight of the modular connector is not included for simplicity. The magnitude of the snow load, N is 0.666 kN/m^2 (13.9 psf), calculated per the design code assuming that the structure is a flat roof (ASCE/SEI, 2017). The snow load is calculated based on the projected area of the structure. Both the dead and snow loads are applied as point loads at the free nodes.

For each span length, the grid shell with the lowest weight is shown in Figure 10. Spans S_2, S_3, and S_4 have similar forms, while span S_1 requires less number of members to achieve the desired span length. Table 1 contains summarized results including: the lowest weight, W_{min}, mesh size, h, the z-coordinate of the center node, z_c, largest axial force, F_{max}, member buckling capacity factor, $\mu = \max(F/U)$, member section size, and the lowest eigenvalue, λ_1.

For all four spans, the methodology selects two of the largest section sizes in the database, W14x233 for S_1 and W14x257 for the other three. This is primarily to satisfy the global system buckling constraint of $\lambda_1 \geq 1$. Both section sizes have a large stiffness in their weak axis resulting in a significant compressive capacity in each member, while the axial forces in the members are much lower in comparison. This is indicated by the lower value of the member buckling capacity factor, μ.

To further demonstrate how the proposed methodology finds the grid shell with the lowest weight, the change in z_c based on self-weight, W, peak axial force, F_{max}, critical buckling load factor, λ_1, and member buckling capacity factor, μ is traced for different values of the scale factor, ξ for the case study S_2 = 53.3 m (175 ft) and mesh size h = 9.14 m (30 ft) in Figure 11. It is evident that deeper grid shells have a higher structural weight as the length of the truss elements increase (Figure 11A). However, higher values of z_c lower the peak axial force and thus, increase the global system buckling capacity as λ_1 becomes considerably higher than the requirement (Figure 11B and C). The results in Figure 11D indicate that the member buckling constraint does not govern the selection of the grid shell form, as the factors, μ for each value of ξ are significantly lower than 1. For shallower grid shells, the largest section size is selected and a low value of μ results. As z_c increases, axial forces decrease and smaller section sizes are selected with μ also increasing, until the smallest section size of W14x109 is chosen. From there, with increasing z_c, the member forces and thus, also μ continue to decrease. Overall, to minimize the weight of the structure, the methodology selects a form that has a low structural depth and the largest wide flange section size to achieve λ_1 close to the requirement of 1.

For span S_2, a total of 100 scale factors ξ were investigated. However, only 27, in the range between 80 and 300, were found to result in feasible solutions, as shown in Figure 11. The lower bound of the factor ξ is primarily controlled by geometric constraints as deeper grid shells increase both the angles, γ and the member lengths, L_m. The upper bound of ξ, however, is governed by the structural constraints, as too shallow of grid shells significantly lower both member and global system buckling capacity.

From all 31 mesh sizes, h investigated for each span length, not all result in feasible solutions.

Figure 12 shows the mesh sizes, h that result in feasible solutions for all span lengths. The reduced number of mesh sizes is primarily due to the system buckling constraint as grid shells with a form diagram type Γ_2 resulted in a significantly low eigenvalues λ_1, and thus insufficient buckling capacity.

DEMONSTRATION OF FEASIBILITY

Grid shell structures can experience different buckling modes including member buckling, node buckling (snap-through buckling), torsional buckling of the node, and global buckling (Gioncu, 1995). The nodal connector, particularly in single layer grid shells, has a significant importance on the global stability of the structure. There is extensive research on buckling of grid shells and other space frame structures that takes into account the nodal connector, initial imperfections, and geometric and material nonlinearity. Suzuki et al. (1992) investigated the effect of material and geometric nonlinearity on the buckling behavior of single layer reticulated domes with rigidly connected members. Kato et al. (1998) studied the collapse behavior of domes with semi-rigid nodal connectors, incorporating initial imperfections. The collapse mechanism of single layer domes is significantly influenced by both the geometry of the structure and the connector's stiffness. Lopez et al. (2007a) proposed an approach to determine the buckling load of domes with semi-rigidly connected members for various loading condition and geometric parameters. Additionally, Lopez et al. (2007b) conducted numerical and experimental studies in which the node stiffness, member properties, and load distribution were incorporated to determine the critical buckling load. Hwang (2010) numerically investigated the impact of the connector's stiffness and initial imperfections on the buckling of the grid shells. The study showed that the structure can experience failure under relatively low loads as a result of bending stresses which lower the stiffness of the joint.

Given the importance of global stability in grid shell design, this research demonstrates the feasibility of the modular connector and the developed forms through 3D FE linear eigenvalue buckling analyses in the software package ABAQUS/Standard (ABAQUS, 2016) (Figure 13). The modular connectors and the wide flange sections are modeled using 4-node (S4R) or 3-node (S3R) reduced integration general purpose shell elements with six degrees of freedom. A 50.8-mm (2-

in.) mesh size, determined through mesh refinement studies, was used for all components. The tension tie is not modeled for simplicity. Instead, the outer wide flange members are connected to horizontal wide flange segments, representing what could be a final boundary modular connector. At the end of each of the wide flange segments at the node intersecting the web and bottom flange, the following boundary conditions are applied: translation is restrained in all three orthogonal directions, free rotation in all directions. The bolted splices are not modeled explicitly. Instead all nodes along the edges of the flanges of the members are tied to the nodes along the edges of the flanges of the modular connectors or the horizontal wide flange segments. Similarly, the nodes along the web edge of the members are tied to the nodes along the web edge of the modular connector or the horizontal wide flange segments. The constraint ties all degrees of freedom at the nodes throughout the duration of the analysis. Grade 50 structural steel properties are assumed: 345 MPa (50 ksi) minimum yield strength, 200 GPa (29000 ksi) modulus of elasticity, 7850 kg/m^3 (490 lbs/ft^3) steel density, and 0.3 poisson's ratio.

The linear eigenvalue buckling analysis was performed for case study S_2 = 53.3 m (175 ft) and load scenario I_2 (highest magnitude of the load). In this model, the self-weight of all structural steel components was applied through the specific density and the acceleration of gravity. Both, self-weight of the structural glass and snow load were applied as a point load at every elemental node along the middle line of the top flange of the wide flange members. Members were modeled using the W14x257 section size determined earlier through the proposed methodology. Based on this section size, the thickness of the flange plates as well as the thickness of the web plates in the modular connectors were selected to be the same as for the wide flange members. The HSS size was HSS16x0.625. The thickness of the flanges as well as the thickness of the web of the horizontal wide flange segments were selected to be the same as the modular connector. The length of the each segment was: $l_s = e + c$. These parameters of the modular connectors, the horizontal wide flange segments, and HSS could also be determined based on other structural constraints as well as using optimization approaches.

Figure 14 shows the buckling mode shape of the structure corresponding to the critical load factor, that is the smallest eigenvalue of 5.1 determined from the FE analyses. As the load is multiplied by this critical load factor, the structure experiences global buckling as shown in Figure 14. This mode shape is expected due to the parabolic, arch-type geometry of the grid shell. The considerably high critical load factor indicates a significant increase in the system buckling capacity in comparison to the results from the form-finding methodology from which the critical load factor is 1. This difference can be attributed to the fact that TNA uses truss elements with no rotational stiffness and the modular connectors were not modeled. In contrast, in the FE analysis, the moment-resisting connection between the members and modular connectors is incorporated through the tie constraints. By explicitly modeling the modular connectors, the eccentricity of loading due to the starter segments is incorporated as well (eccentricity was not considered in the form-finding methodology). The high critical load factor indicates a satisfactory performance of the system even with the load eccentricity included. The FE analysis indicates that the novel modular connector provides an enhanced buckling resistance due to the ability to achieve a moment-resisting connection and demonstrates that the proposed form-finding methodology is conservative.

CONCLUSION

This paper proposed a new modular approach to address a major challenge in the design, fabrication and erection of steel grid shells: the nodal connector. More specifically, this research introduces a novel modular connector which can be easily prefabricated and readily available. A single modular connector can be used to achieve various grid shell forms. Thus, this paper proposed a new kit-of-parts approach comprised of: (1) prefabricated modular connectors, (2) standard wide flange sections, and (3) bolted splice connections that can be used for both free-form and form-found grid shells. This approach also provides a significant structural advantage as it achieves a moment-resisting connection allowing the load to be redistributed in case of a sudden member loss or replacement.

In this research, a new paradigm in design of steel grid shells was proposed: start with the nodal connector that is designed for ease of fabrication and then develop efficient structural forms that are consistent with the connector. Specifically, the development of free-form grid shells using the kit-of-parts was first introduced. Additionally, a methodology for finding efficient grid shells that are compatible with the modular connector was proposed. By using a numerical form-finding technique that is consistent with the modular connector, coupled with structural and geometric constraints, the methodology develops a compression-only grid shells and selects the section size of the wide flange members while minimizing the self-weight of the structure. Linear eigenvalue buckling analyses using a high-fidelity FE numerical model were performed to investigate the global behavior of the developed structures. The results demonstrated the promise of the modular connector to achieve efficient forms while providing enhanced stability to the structure through the moment-resisting connection.

This research has focused on conceptually designing the modular connector, developing the form-finding methodology, and demonstrating the feasibility of the found forms through linear eigenvalue buckling analysis. Future research could focus on shape and sizing optimization of the modular connector. For example, a multi-objective optimization problem could be formulated to include material efficiency and fabrication/erection cost while meeting structural and transportation requirements. Additionally, prefabrication and construction strategies could be explored and the behavior of the system during erection should be investigated. A prototype could be built for better understanding the behavior of the system under construction and design loads. As the modular connector uses moment-resisting connections, there is a potential for the system to sustain higher loads, tolerate sudden member loss, and permit member replacement without compromising its structural integrity. Analysis to understand these behaviors would require a refinement of the the FE model to include material and geometric nonlinearities. A nonlinear material model can be incorporated, for example assuming an elastic-perfectly plastic stress-strain relationship or if needed, including strain hardening. The sudden member loss scenario can be simulated using different FE models, for example: (1) a member is severed, and dynamic analysis is performed that can capture the high velocity stress wave propagation through the wide flange member into the connector and (2) member is removed from the geometry and nonlinear static analysis is performed to investigate the behavior of the faulted structure. The second analysis could be used for evaluating the structure for member replacement.

Ultimately, this research presents a new approach to the design of steel grid shell structures that "modularizes" the nodal connector between members allowing identical modular connectors to be used repeatedly throughout the structure and among many structures. This approach aims to reduce the time and cost for fabrication and erection, while also achieving a resilient structural design.

DATA AVAILABILITY STATEMENT

Some or all data, models, or code that support the findings of this study are available from the corresponding author upon reasonable request.

ACKNOWLEDGMENTS

This material is based upon work supported by the National Science Foundation under Grant No. CMMI-1351272. Mirela D. Tumbeva is also supported by the O.H. Ammann Research Fellowship. Support from these sources and the program managers is gratefully acknowledged. Contributions from Ted Zoli, the National Bridge Chief Engineer of HNTB Contribution, are also gratefully acknowledged.

REFERENCES

ABAQUS (2016). *ABAQUS/Standard Analysis User's Manual Version 6.14*. Dassault Systemes, Waltham, MA.

S. Adriaenssens, P. Block, D. Veenendaal, and C. Williams, eds. (2014). *Shell Structures for Architecture: Form Finding and Optimization.* Routledge.

Adriaenssens, S. M. L. and Barnes, M. R. (2001). "Tensegrity spline beam and grid shell structures." *Engineering Structures*, 23(1), 29–36.

AISC (2011). *Steel Construction Maunal*. American Institute of Steel Construction (AISC), Chicago, IL, 14th edition.

Allred, III, J. B., Griswold, M. D., Hall, J. M., Bush, M., and Kummer, J. (2013). “3-dimensional universal tube connector system, U.S. Patent No. 8528291.

ASCE/SEI (2017). *Minimum Design Loads and Associated Criteria for Buildings and Other Structures, ASCE/SEI 7-16*. American Society of Civil Engineers (AISC), Structural Engineering Institute, Reston, VA, 16 edition.

Bagrianski, S. and Halpern, A. B. (2014). “Form-finding of compressive structures using prescriptive dynamic relaxation.” *Computers and Structures*, 132, 65–74.

Barnes, M. R. (1988). “Form-finding and analysis of prestressed nets and membranes.” *Computers and Structures*, 30(3), 685–695.

Barnes, M. R. (1999). “Form finding and analysis of tension structures by dynamic relaxation.” *International Journal of Space Structures*, 14(2), 89–104.

Block, P. (2009). “Thrust network analysis: Exploring three-dimensional equilibrium.” Ph.D. thesis, Massachusetts Institute of Technology, Cambridge, MA.

Block, P. and Ochsendorf, J. (2007). “Thrust network analysis: A new methodology for three-dimensional equilibrium.” *Journal of the International Association for Shell and Spatial Structures*, 48(3), 1–8.

Boots, A. H. (2008). “Spherical hub for modular structural system, U.S. Patent No. 0016789.

Day, A. S. (1965). “An introduction to dynamic relaxation.” *The Engineer*, 219, 218–221.

Feng, R., Ye, J., and Zhu, B. (2015). “Behavior of bolted joints of cable-braced grid shells.” *Journal of Structural Engineering*, 14(12), 04015071.

Fraternali, F. (2010). “A thrust network approach to the equilibrium problem of unreinforced masonry vaults via polyhedral stress functions.” *Mechanics Research Communications*, 37(2), 198–204.

Gerbo, E. J., Thrall, A. P., Smith, B. J., and Zoli, T. P. (2016). "Full-field measurement of residual strains in cold bent steel plates.." *Journal of Constructional Steel Research*, 127, 187–203.

Gerbo, E. J., Thrall, A. P., and Zoli, T. P. (2020a). "Adjustable bolted steel plate connection: Measured behavior of bolts during field installation and numerical parametric investigation." *Journal of Structural Engineering*, 146(2), 04019189.

Gerbo, E. J., Thrall, A. P., and Zoli, T. P. (2020b). "Service and ultimate behavior of adjustable bolted steel plate connections." *Journal of Structural Engineering*, 146(7), 04020128.

Gerbo, E. J., Wang, Y., Tumbeva, M. D., Thrall, A. P., Smith, B. J., and Zoli, T. P. (2018). "Behavior of an adjustable bolted steel plate connection during field installation." *Journal of Structural Engineering*, 144(3), 04017223.

Gioncu, V. (1995). "Buckling of reticulated shells: State-of-the-art." *International Journal of Space Structures*, 10(1), 1–46.

Glymph, J., Shelden, D., Ceccato, C., Mussel, J., and Schober, H. (2004). "A parametric strategy for free-form glass structures using quadrilateral planar facets." *Automation in Construction*, 13(2), 187–202.

Hwang, K. J. (2010). "Advanced investigations of grid spatial structures considering various connection systems." Ph.D. thesis, University of Stuttgart, Stuttgart, Germany.

ISO (2013). *ISO 668: Series 1 freight containers - Classification, dimensions, ratings.* ISO, Switzerland, 6th edition.

Kato, S., Mutoh, I., and Shomura, M. (1998). "Collapse of semi-rigidly jointed reticulated domes with initial geometric imperfections." *Journal of Constructional Steel Research*, 48, 145–168.

Knippers, J. and Helbig, T. (2009). "Recent developments in the design of glazed grid shells." *International Journal of Space Structures*, 24(2), 111–126.

Liew, A., Pagonakis, D., Van Mele, T., and Block, P. (2018). “Load-path optimisation of funicular networks.” *Meccanica*, 53(1), 279–294.

Linkwitz, K. and Schek, H.-J. (1971). “Einige bemerkungen zur berechnung von vorgespannten seilnetzkonstruktionen.” *Ingeniuer-Archiv*, 40(3), 145–158.

Lopez, A., Puente, I., and Serena, M. A. (2007a). “Direct evaluation of the buckling loads of semi-rigidly jointed single-layer latticed domes under symmetric loading.” *Engineering Structures*, 29, 101–109.

Lopez, A., Puente, I., and Serena, M. A. (2007b). “Numerical model and experimental tests on single-layer latticed domes with semi-rigid joints.” *Engineering Structures*, 85, 360–374.

Ma, H., Ren, S., and Fan, F. (2016a). “Experimental and numerical research on a new semi-rigid joint for single-layer reticulated structures.” *Engineering Structures*, 126, 725–738.

Ma, H., Ren, S., and Fan, F. (2016b). “Parametric study and analytical characterization of the bolt–column (bc) joint for single-layer reticulated structures.” *Engineering Structures*, 123, 108–123.

Marmo, F. and Rosati, L. (2017). “Reformulation and extension of the thrust network analysis.” *Computers and Structures*, 182, 104–118.

Maxwell, J. C. (1864). “On reciprocal figures and diagrams of forces.” *The London, Edinburgh, and Dublin Philosophical Magazine and Journal of Science*, 27(182), 250–261.

Miki, M. and Kawaguchi, K. (2010). “Extended force density method for form finding of tension structures.” *Journal of the International Association for Shell and Spatial Structures*, 51, 291–303.

Oh, J., Ju, Y. K., Hwang, K., Kim, S., and Lho, S. (2016). “Free node for a single layer free-form envelope subjected to bending moment.” *Engineering Structures*, 106, 25–35.

Panozzo, D., Block, P., and Sorkine-Hornung, O. (2013). “Designing unreinforced masonry models.” *Association for Computing Machinery*, 32(4), 0730–0301.

Reynolds, A. G., Hackbarth, D. R., and Curtis, G. N. (2006). “Connection node for a unversal truss joint and double layer grid, U.S. Patent No. 0053726.

Richardson, J. N., Adriaenssens, S. M. L., Coelho, R. F., and Bouillard, P. (2013). “Coupled form-finding and grid optimization approach for single layer grid shells.” *Engineering Structures*, 52, 230–239.

Rippmann, M. (2016). “Funicular shell design: Geometric approaches to form finding and fabrication of discrete funicular structures.” Ph.D. thesis, ETH Zurich, Zurich.

Rippmann, M., Lachauer, L., and Block, P. (2012). “Rhinovault - interactive vault design.” *International Journal of Space Structures*, 27(4), 219–230.

Rochas, A. (2014). “Universal node for space frame structures, U.S. Patent No. 8820025.

Sanchez, J., Serna, M. A., and Morer, P. (2007). “A multi-step force–density method and surface-fitting approach for the preliminary shape design of tensile structures.” *Engineering Structures*, 29(8), 1996–1976.

Schek, H.-J. (1974). “The force density method for form finding and computation of general networks..” *Computer Methods in Applied Mechanics and Engineering*, 3, 115–134.

Schlaich, J. and Schober, H. (2005). “Freeform glass roofs.” *Structures Congress*, Cambridge, MA, 1–13.

Seifi, H., Javan, A. R., Xu, S., Y., Z., and M., X. Y. (2018). “Desing optimization and additive manufacturing of nodes in gridshell structures.” *Engineering Structures*, 160, 161–170.

Suzuki, T., Ogawa, T., and Ikarashi, K. (1992). “Elasto-plastic buckling analysis of rigidly jointed single layer reticulated domes.” *International Journal of Space Structures*, 7(4), 363–368.

Tumbeva, M. D., Thrall, A. P., and Zoli, T. P. (2018). "Modualr joint for free-form undulating structures." *Proceedings of IASS Annual Symposia*, Vol. 2018, Cambridge, MA, 1–4.

Tumbeva, M. D., Thrall, A. P., and Zoli, T. P. (2021). "Modular joint for the accelerated fabrication and erection of steel bridges." *Journal of Bridge Engineering*, In Press.

Veenendaal, D. and Block, P. (2012). "An overview and comparison of structural form finding methods for general networks." *International Journal of Solids and Structures*, 49(26), 3741–3753.

Ye, J., Feng, R., Zhou, S., and Tian, J. (2012). "The modified force-density method for form-finding of membrane structures." *International Journal of Steel Structures*, 12(3), 299–310.

List of Tables

TABLE 1. Results of the case studies.

S (m)	W_{min} (kN)	h (m)	z_c (m)	F_{max} (kN)	μ	Section size W14x	λ_1
45.7	1699	14.6	2.86	2078	0.253	233	1.01
53.3	2648	9.14	1.62	3049	0.246	257	1.02
61.0	3269	10.4	2.04	3500	0.317	257	1.05
76.2	4713	13.4	2.84	4762	0.505	257	1.02

List of Figures

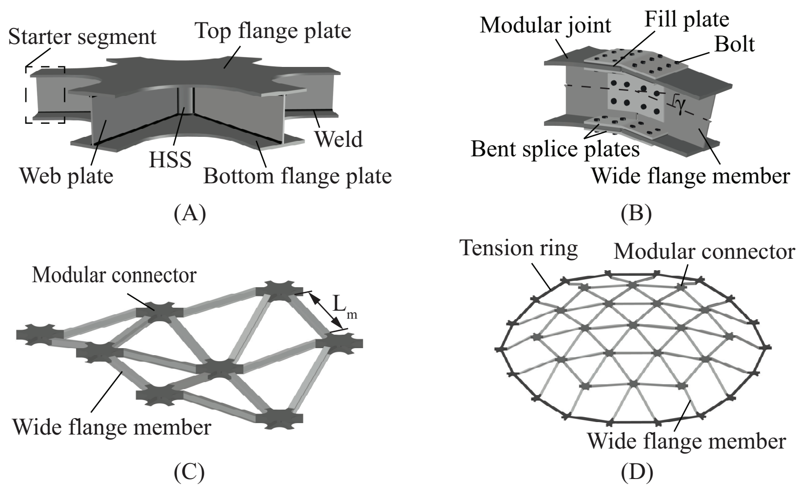

FIG. 1. Modular approach to grid shells: (A) Modular connector, (B) Bolted splice connection, (C) Free-form grid shell, and (D) Form-found grid shell.

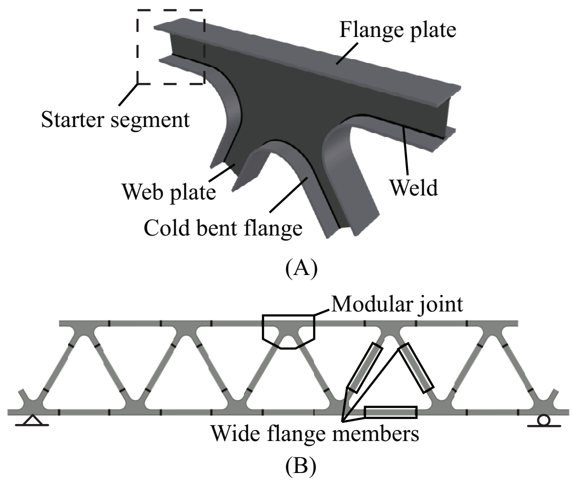

FIG. 2. Modular approach to steel bridges: (A) Modular joint and (B) Constant-depth simply supported bridge with modular joints and standard wide flange members (adapted from Tumbeva et al. (2021), ©ASCE).

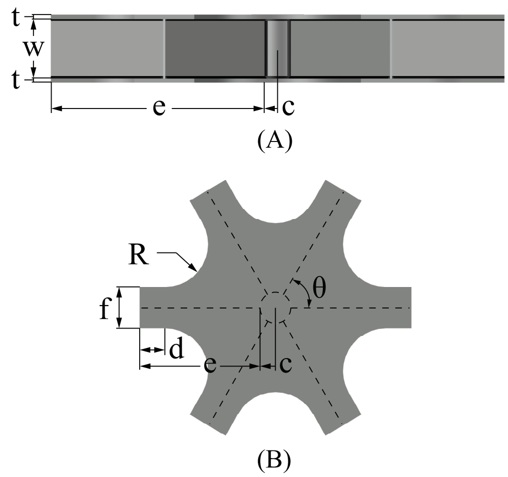

FIG. 3. Geometric parameters of the modular connector: (A) Elevation view and (B) Plan view.

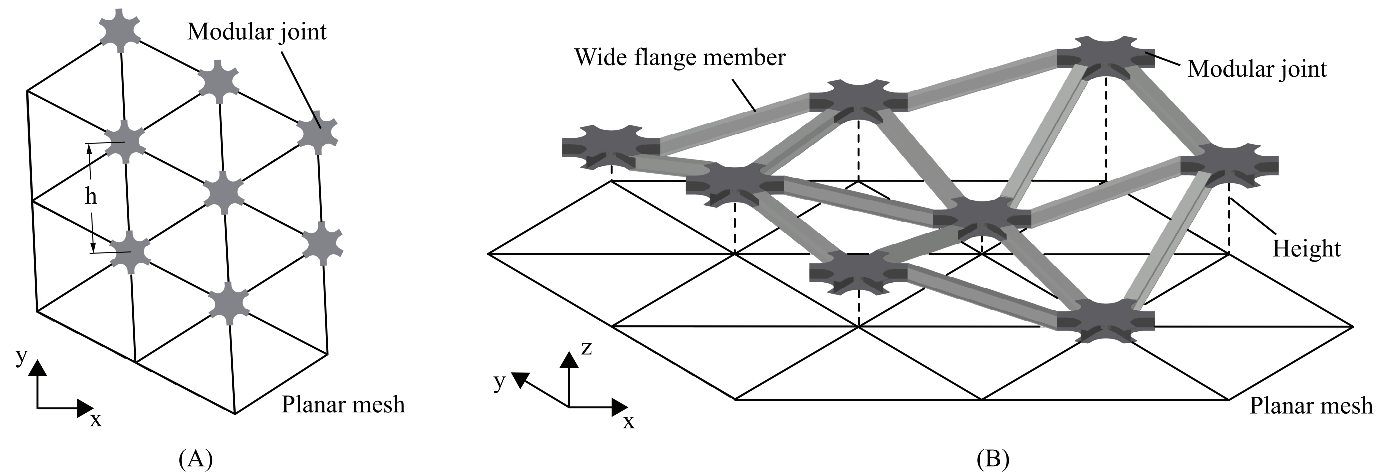

FIG. 4. Free-form grid shell: (A) Modular connectors projected onto a parallel planar mesh and (B) Isometric view of modular connectors connected to wide flange members (splice plates not shown for clarity) [(A) and (B) adapted from Tumbeva et al. (2018)].

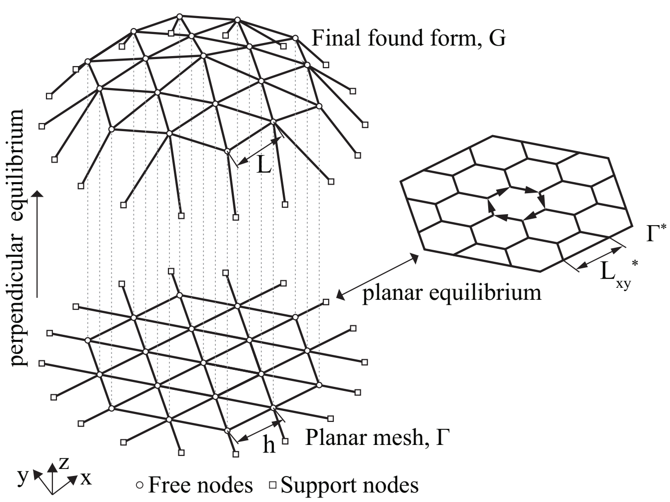

FIG. 5. Form-found 3D equilibrium network, G, its planar projection the form diagram, Γ, and the reciprocal force diagram, Γ^*.

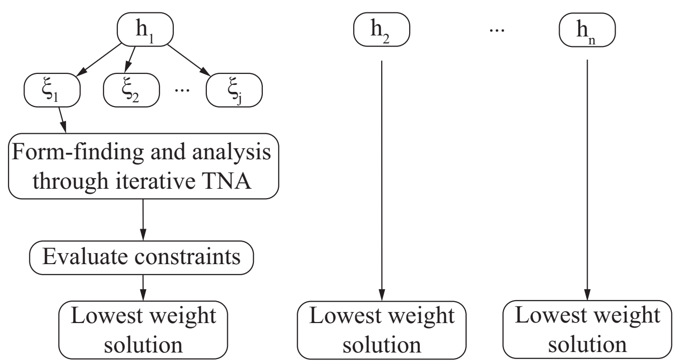

FIG. 6. Compression-only form-finding methodology overview.

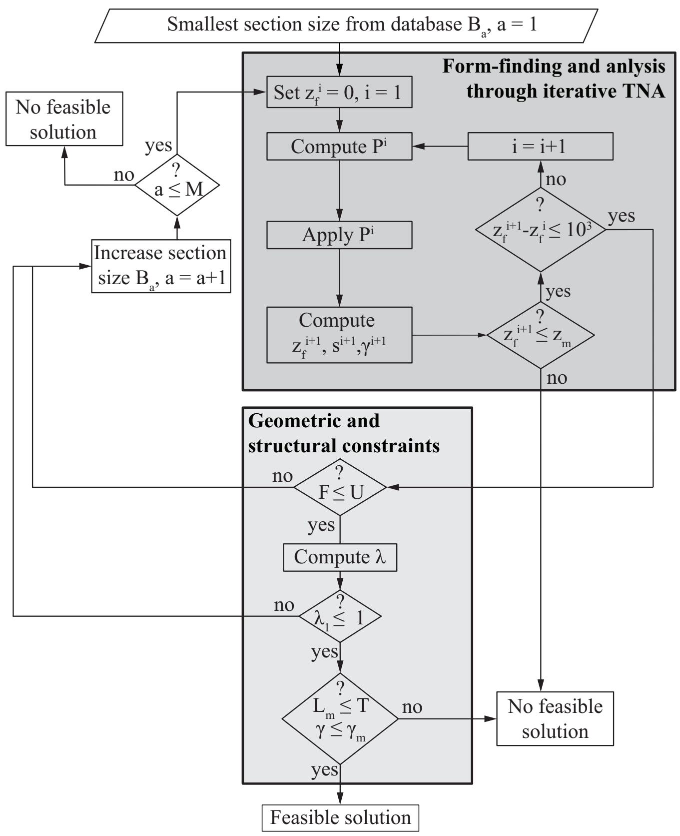

FIG. 7. Flow chart of the form-finding methodology for single combination of h and ξ.

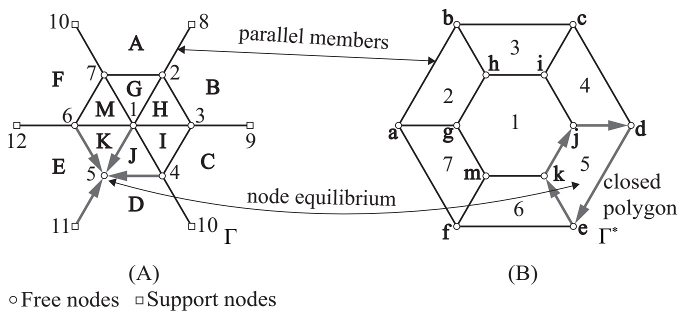

FIG. 8. Reciprocal diagrams: (A) Form diagram, Γ and (B) Force diagram, Γ^*.

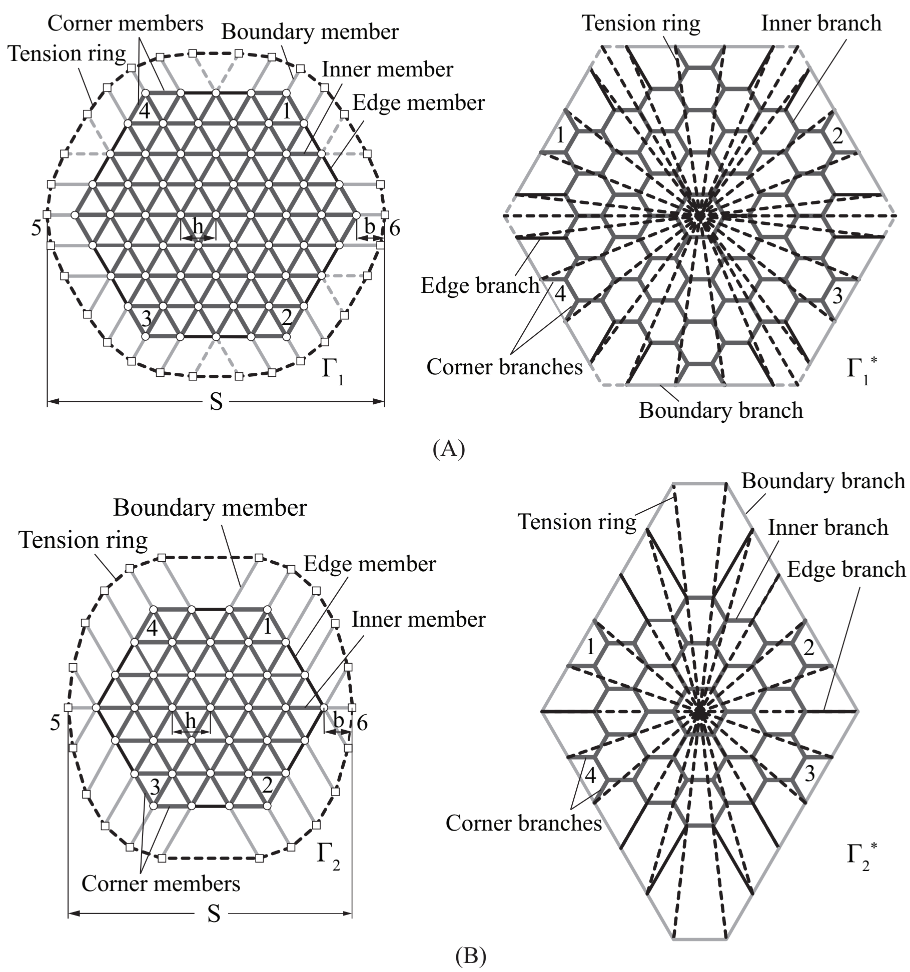

FIG. 9. Development of form and force diagrams: (A) Type Γ_1, Γ_1^* and (B) Type Γ_2, Γ_2^*.

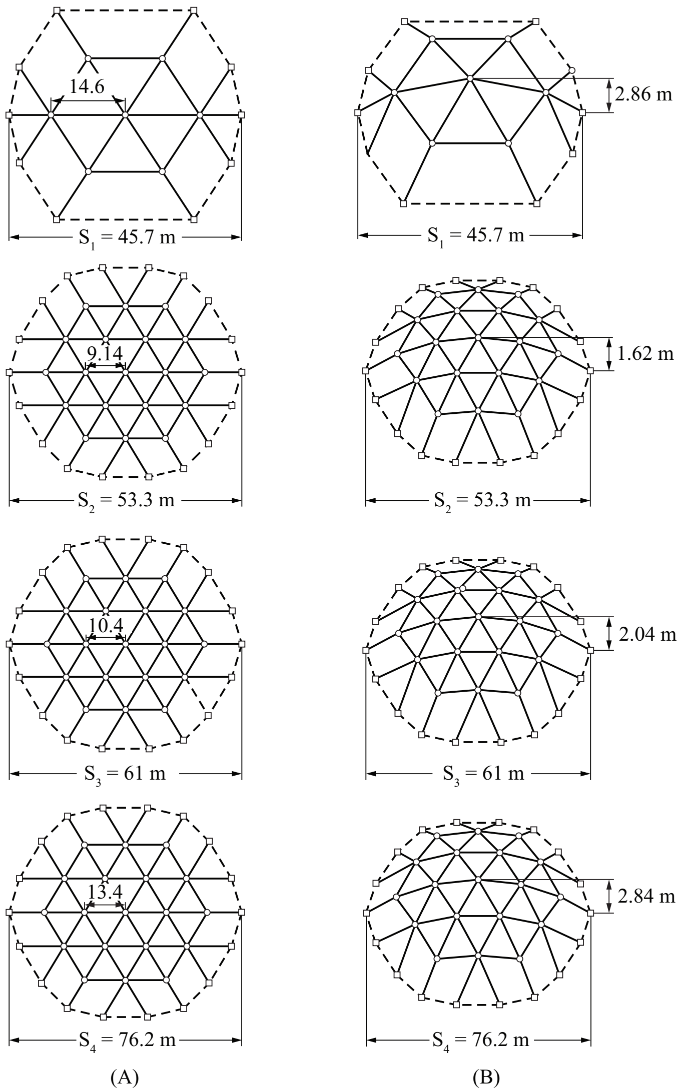

FIG. 10. Results for each case study: (A) Planar mesh, the form diagram, Γ and (B) Form-found grid shell, G (not drawn to scale).

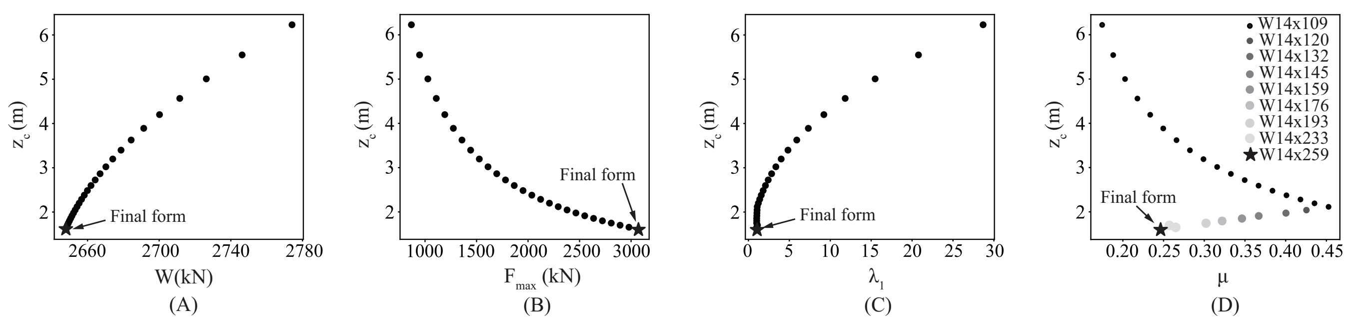

FIG. 11. Results for S_2 = 53.3 m and h = 9.14 m based on: (A) Weight, W, (B) Largest axial force, F_{max}, (C) critical buckling load factor, λ_1, and (D) member buckling capacity factor, μ.

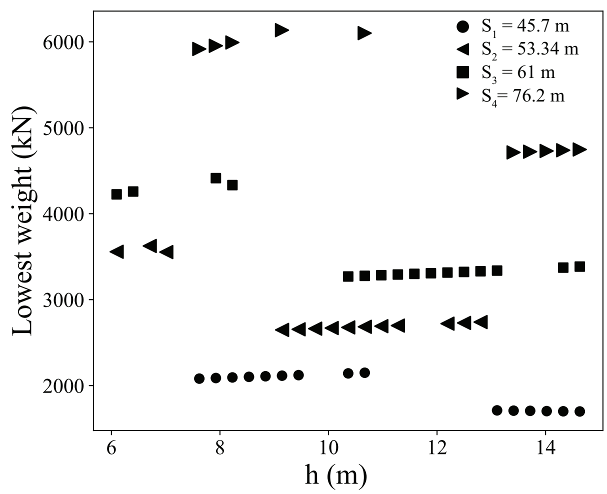

FIG. 12. Lowest weight solution for each mesh size, h.

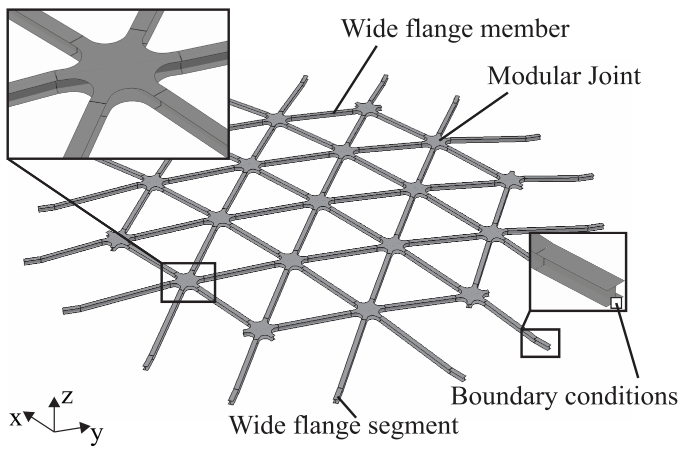

FIG. 13. Finite element model.

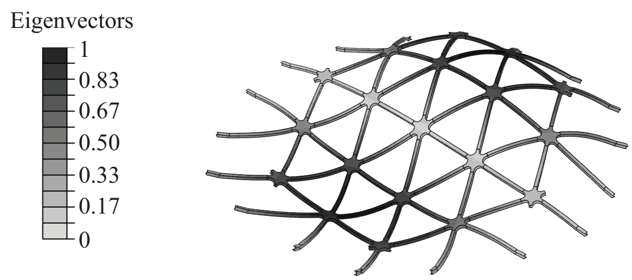

FIG. 14. Buckling mode shape corresponding to critical load factor of 5.1 determined from 3D FE linear eigenvalue analysis for span S_2 = 53.3 m and h = 9.14 m.